VARIABLE FREQUENCY CONTROL FOR SPIDER-DRIVEN ULTRA-PRECISION STAGES

Seiji Hashimoto [*,1] **Kiyoshi Ohishi** [**]
Koji Kosaka [***] **Takeo Ishikawa** [*]
Hiroshi Kubota [****] **Tadahiro Ohmi** [†]

[*] *Gunma University, Japan*
[**] *Nagaoka University of Technology, Japan*
[***] *Kumamoto Technology Inc., Japan*
[****] *Kumamoto University, Japan*
[†] *Tohoku University, Japan*

Abstract: This paper proposes a variable control method of drive frequency for the SPIDER-driven precision stage. Control performances such as positioning accuracy and maximum velocity strongly depend on the drive frequency. At first, the identification experiments of the SPIDER with different drive frequency are carried out. Next the gain-scheduled control strategy for the variable frequency control, considering the variation rate of the frequency is introduced. Finally, simulations and experiments are performed in order to verify the efficiency of the proposed control method.

Keywords: ultra-precision stage, variable-frequency drive, scheduled $\mathcal{H}_\infty$ control, precision positioning

1. INTRODUCTION

The authors have reported the continuous-path tracking method of the SPIDER (Synchronous piezoelectric device driver)-driven precision stage (Hashimoto *et al.*, 2004). The SPIDER is the novel actuator developed by Kumamoto Technology Inc., which uses the nonresonant characteristic of an ultrasonic motor. The SPIDER-driven stage has many potential applications to future LSI manufacturing, in particular electron beam technologies because of the advantages of high resolution, no magnetic noise generation, high servo rigidity and high retention. The SPIDER which has eight legs with the pre-load mechanism is shown in Fig. 1. Table 1 shows the characteristics of the actuator used in this study.

In the previous research, the amplitude of the applied voltage was selected as the control input in which the drive frequency was constant. The frequency variable is one of the original features of the SPIDER, something that was impossible in the conventional resonant-type actuator.

In this paper, the novel control technique considering the ability of changing the drive frequency is proposed for the SPIDER-driven stage control and it's effectiveness is verified through simulations and experiments.

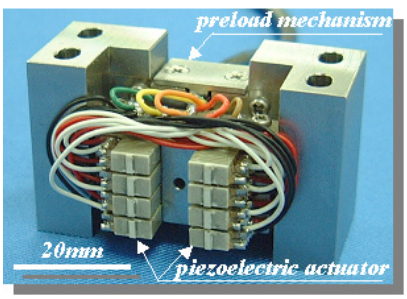

Fig. 1. Nonresonant ultrasonic motor(SPIDER).

[1] Partially supported by the Grant-in-Aid for Scientific Research from JSPS

Table 1. Actuator properties.

Material	$Pb(Zi, Ti)O_3$
Density	7.8×10^3 [kg/m^3]
Dimension	$6.0 \times 3.0 \times 0.6$ [mm]
Expand mode	660×10^{-12} [m/V]
Shear mode	1010×10^{-12} [m/V]

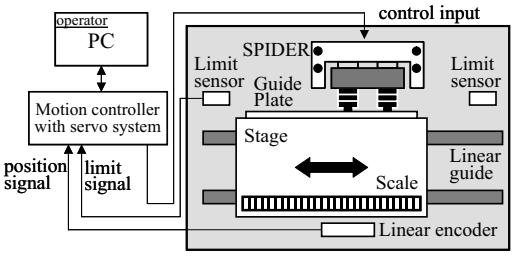

Fig. 2. Experimental setup for SPIDER-driven stage.

2. DRIVE FREQUENCY CHARACTERISTIC OF SPIDER

A simplified experimental setup of the investigated SPIDER-driven precision stage is presented in Fig.2. The drive sequence of the SPIDER is given in Fig.3. One leg is structured by eight-stacked piezoelectric plates, the upper four plates are for the expand motion and the bottom four are the shear motion. The friction tip of the SPIDER contacts the plate at the side of the stage. The elliptical drive orbit of the tip become possible by applying a sine wave drive for both expand and shear motions. The phase difference between two motions is $\pi/2$ rad, and that between two legs is π rad.

The velocity characteristic of the SPIDER-driven precision stage is illustrated in Fig.4. The steady state velocity for a control input of 1 V is plotted against the drive frequency. From this figure, it is noticed that the stage velocity increases linearly with the drive frequency. The drive frequency of the conventional actuator, which uses piezoelectric material, is limited to the resonant frequency because of the large gain obtained only at that frequency. The utilization of the resonant frequency brings problems such as time lag, velocity deviation and positioning resolution. In this actuator, a drive with nonresonant frequency is possible because of the features of the operation principle(Egashira *et al.*, 2004). Therefore, these problems can be overcome by the nonresonant frequency drive. In addition, the excellent control becomes possible by employing a drive frequency variable control.

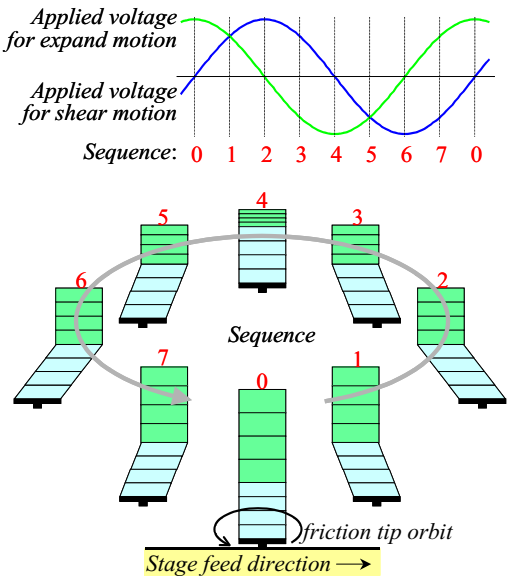

Fig. 3. Drive sequence of the SPIDER.

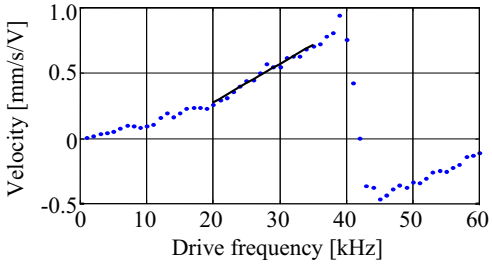

Fig. 4. Velocity characteristic for drive frequency.

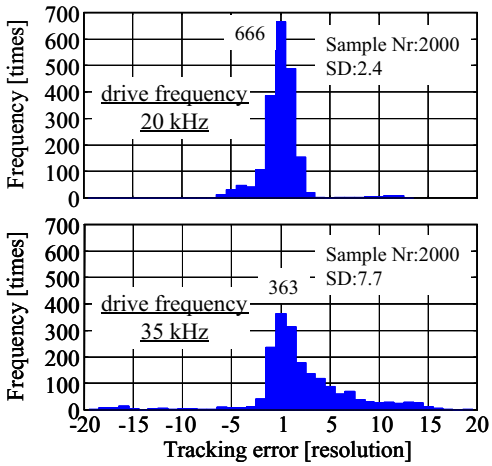

Fig. 5. Comparison of tracking performance.

One example of the advantages of introducing a variable control of the drive frequency is described below; Experiments for a constant velocity control with a dive frequencies of 20 kHz and 35 kHz were carried out. A position control system with a control bandwidth of 100 Hz was designed by means of the PID control. Fig. 5 shows the histogram of the tracking error to the ramp position reference with 10 mm/s inclination. Even though the maximum velocity is getting smaller with respect to the decrease of the drive frequency as shown in Fig.4, the velocity deviation can be decreased. From these results, the control techniques considered are:

- to lower the drive frequency as much as possible
- to carries out a variable-frequency drive in accordance with a reference orbit

In this paper, we focus on the variable-frequency drive from a frequency of 20 kHz up to 35 kHz.

Another important aspect is that a variable frequency control has the possibility of the slip reduction between the friction tip and the contacting plate(Egashira *et al.*, 2004). This can prevent the deterioration of accuracy caused by slide wear.

3. VARIABLE-FREQUENCY DRIVE METHOD

3.1 Modeling of SPIDER

In order to derive the dynamic of the SPIDER-driven stage as well as the velocity characteristic, the identification experiments(Ljung, 1999) are carried out. The input signal is the applied voltage to the SPIDER and the output signal is the position from the encoder which has the resolution of 100 nm. The identified 2^{nd}-order models for 20 kHz and 35 kHz are;

$$P_{20}\ [mm/V] = k_{min} \cdot \frac{1}{s/p_{max}+1} \cdot \frac{1}{s} \quad (1)$$

$$P_{35}\ [mm/V] = k_{max} \cdot \frac{1}{s/p_{min}+1} \cdot \frac{1}{s} \quad (2)$$

where, $k_{min} = 0.259$, $k_{max} = 0.723$, $p_{min} = 96.2$, $p_{max} = 252$. Fig. 6 representatively shows the velocity response of the experimental outputs and the model outputs to step inputs of the same amplitude. To compare the time responses, it is confirmed that the dynamics of the stage are well identified. The identification results of the gain and pole for each drive frequency defined as ω are shown in Fig.7. From these figures, it is noticed that the change of the drive frequency results in the structural change of the considered plant.

3.2 Gain-Scheduled Controller Design

In order to enhance the dynamic performances of the designed system by changing the drive frequency, the gain-scheduled $\mathcal{H}_\infty$ control strategy

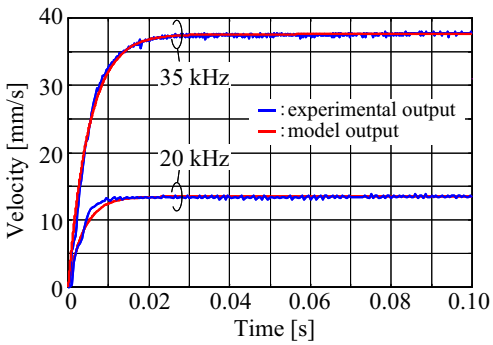

Fig. 6. Comparison of experimental output and model output.

is introduced (Gahinet, 1995). An advantage to introduce the gain-scheduled control is no need an " intermediate " system.

Though the scheduling parameters are both the pole and the gain in this case, considering the combination of those, the parameters and the controller become

$$\Xi = (K_S | K_{Smin} \leq K_S \leq K_{Smax}) \quad (3)$$

$$C(K_S) = \alpha C_{20} + (1-\alpha) C_{35} \quad (4)$$

where, $K_{Smin} = (k_{min}, p_{max})$, $K_{Smax} = (k_{max}, p_{min})$ and $\alpha = (K_S - K_{Smax})/(K_{Smin} - K_{Smax})$. C_{20} and C_{35} are the corresponding controller to P_{20} and P_{35}. Let us define the obtained controllers as biproper transfer function and of minimum phase. Then, the block diagram of the control system including the anti-windup compensation(Goodwin *et al.*, 2001) is illustrated in Fig.8. $C_{[20,35]\infty}$ is the direct feedthrough term and $\bar{C}_{[20,35]}$ a strictly proper transfer function described as:

$$C_{[20,35]}(s) = C_{[20,35]\infty} + \bar{C}_{[20,35]}(s) \quad (5)$$

Moreover, $H_{[20,35]}(s)$ is defined as follows:

$$H_{[20,35]}(s) = [C_{[20,35]}(s)]^{-1} - [C_{[20,35]\infty}]^{-1} \quad (6)$$

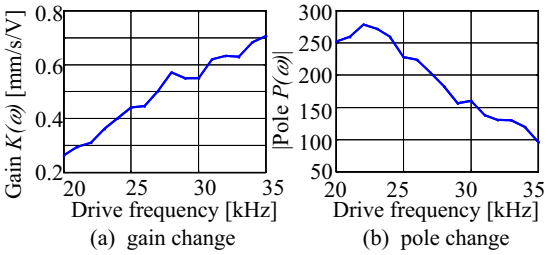

Fig. 7. Gain/pole plots versus drive frequency.

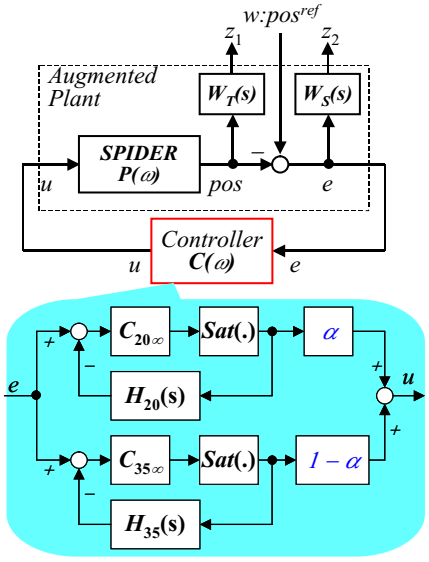

Fig. 8. Block diagram of the gain-scheduled control system.

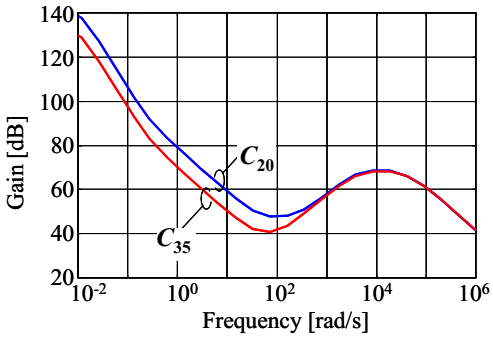

Fig. 9. Controllers' Bode diagram.

The saturation block $Sat(.)$ can be described as:

$$Sat(u(t)) \equiv \begin{cases} u_{max} \;\; if \;\; u(t) > u_{max}, \\ u(t) \;\; if \;\; u_{min} \leq u(t) \leq u_{max}, \\ u_{min} \;\; if \;\; u(t) < u_{min}. \end{cases} \quad (7)$$

Let us define the design specification in terms of overshoot 5 % to step reference as well as no tracking error at steady state to ramp reference. The design concepts of the weighting functions (Doyle *et al.*, 1992) are to satisfy the overshoot, to robust for the gain and the pole uncertainty, and to be of 100 Hz bandwidth. Based on both the control bandwidth and the uncertainty between the real plant and the considered mathematical model, the following weighting function $W_T(s)$ for the multiplicative plant uncertainty has been deduced:

$$W_T(s) = \frac{K_T(T_2 s + 1)}{T_1 s + 1} \quad (8)$$

with $K_T = 0.95, T_1 = 6.67 \cdot 10^{-6}, T_2 = 6.67 \cdot 10^{-4}$.

According with the design procedure for servo system, in order to eliminate the tracking error for steady state we have to increase the maximum singular value of the designed weight $W_S(s)$ in low frequency range. This can be done by shaping the $W_S(s)$ weighting function as:

$$W_S(s) = \frac{K_S}{s^2 + 2\zeta\omega_n s + \omega_n^2} \quad (9)$$

with $K_S = 10^4, \zeta = 1.0, \omega_n = 5 \cdot 10^{-4}$.

The controller can be synthesized using the Matlab LMI Toolbox. The Bode plot of the designed 5^{th}-order controllers C_{20}, C_{35} are shown in Fig.9. It is confirmed that the controller contains the integrator as an internal model.

In order to make the controllers be biproper transfer function, the high-pass filter is convolved to those numerators. Let us note the obtained anti-windup-type controllers by:

$$C_{[20,35]\infty} = [381.9, 381.9] \quad (10)$$

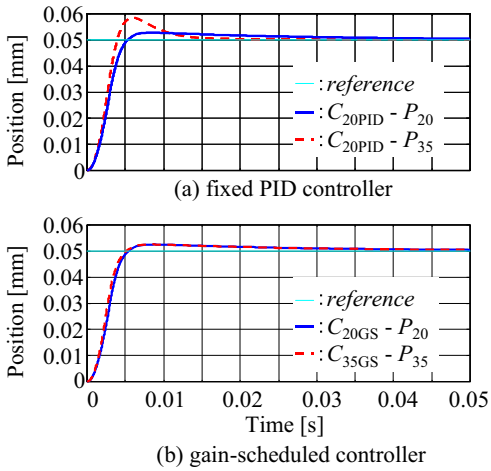

Fig. 10. Step response of the fixed PID and the gain-scheduled control systems.

$$H_{[20,35]}(s) = K_{[20,35]} \frac{\Pi(s - z_{[20,35]})}{\Pi(s - p_{[20,35]})} \quad (11)$$

with
$K_{[20]} = [-705]$,
$z_{[20]} = [-1.51 \cdot 10^5, 101 \pm 49.5i, -0.261]$,
$p_{[20]} = [-3.14{\cdot}10^5, -1.50{\cdot}10^5, -252, -42.6, -0.208]$,
$K_{[35]} = [-702]$, $z_{[35]} = [-1.51{\cdot}10^5, 408, 12.0, -0.203]$,
$p_{[35]} = [-3.14{\cdot}10^5, -1.50{\cdot}10^5, -96.2, -42.6, -0.208]$.

3.3 Simulation and Experimental Verifications

For the comparison, the PID controllers fixed with both models P_{20} and P_{35} were designed in the same position control bandwidth. For the step position reference, the simulation is performed to the drive frequency of both 20 kHz and 35 kHz with the 20 kHz fixed PID controller. The obtained simulation results are illustrated in Fig. 10 (a). From this figure, the deteriorations of the time response especially in the overshoot towards the drive frequency change are seen. The overshoot O_S increases with an increase of the drive frequency (O_S: 5.50 % → 17.0 %).

Fig. 10 (b) shows the time responses of the proposed gain-scheduled control system for 20 kHz and 35 kHz. The performance(O_S:5.05 % → 5.05 %) is improved comparing to that of the fixed PID control system. Furthermore, the Bode diagram for both the control systems is illustrated in Fig.11. From these results, it can be confirmed that the controller positively utilizes information of the drive frequency.

Next, the experiment was carried out in case of 20 kHz and 35 kHz drive frequency as well as the variation of the frequency. Fig. 12 represents the overshoot versus the drive frequency to the step position reference. The control performance can be guaranteed as respected.

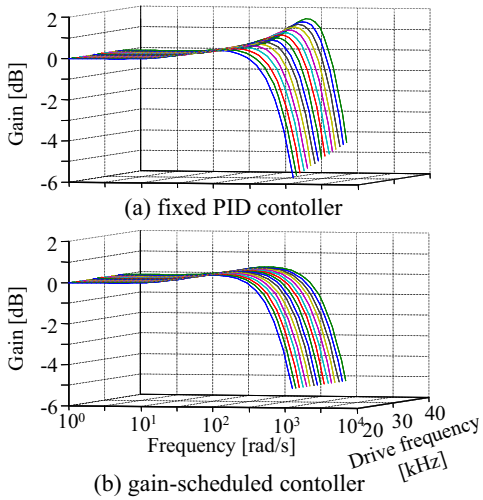

Fig. 11. Gain plots versus drive frequency.

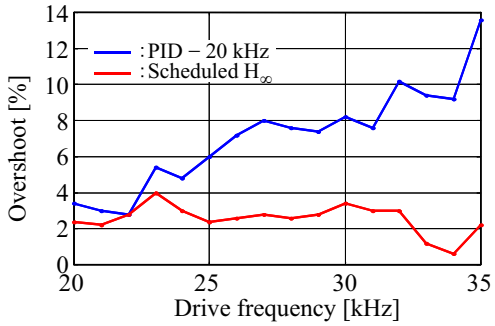

Fig. 12. Experimental results of overshoot to the step position reference.

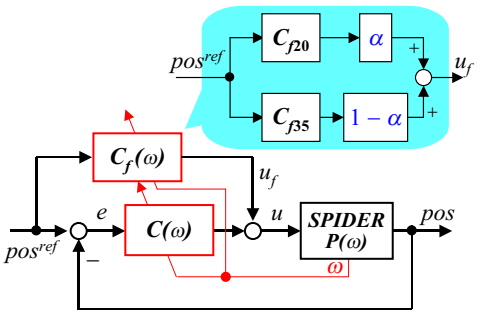

Fig. 13. Block diagram of the gain-scheduled CPTC system.

4. CONTINUOUS-PATH TRACKING FOR VARIABLE-FREQUENCY DRIVE

4.1 Continuous-Path Tracking

In this section, the application of the variable frequency drive described above to a continuous-path tracking control (CPTC) system is shown. The block diagram of the system is illustrated in Fig. 13. The continuous-path tracking controller $C_f(s)$ consists of the plant model and a low-pass filter with sufficiently large bandwidth as:

$$C_f(s)[V/mm] = [P_{[20,35]}(s)]^{-1}F(s) \qquad (12)$$

$F(s)$ is 2^{nd} order and has the bandwidth of 5,000 Hz. $C_f(s)$ is also scheduled in accordance with

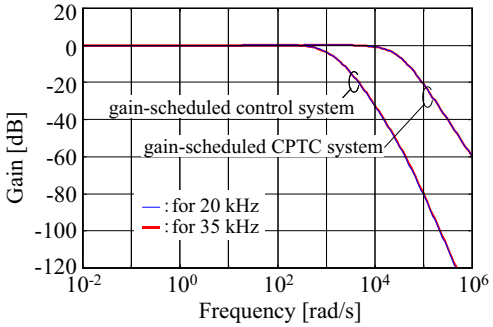

Fig. 14. Bode plot of the gain-scheduled CPTC system.

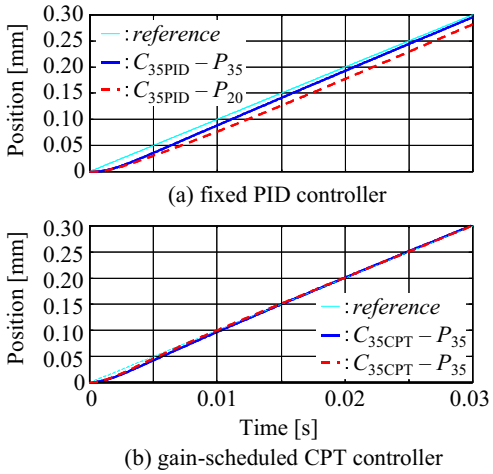

Fig. 15. Ramp response of the fixed PID control and the gain-scheduled CPTC systems.

the drive frequency. The Bode plot for the gain-scheduled CPTC system as well as the gain-scheduled control system described in the previous section for the 20 kHz drive frequency is shown in Fig. 14.

Next, the ramp position reference with the rate of 10 mm/s is applied to both the fixed PID control system and the gain-scheduled CPTC system. Fig. 15 (a) shows time responses for the 35 kHz fixed PID control system to the 35 kHz drive frequency as well as 20 kHz. From this figure, the maximum tracking error e_{max} increases with a decreasing of the drive frequency (e_{max}: 14.5 μm → 23.9 μm). In case of the proposed CPTC system presented in Fig. 15 (b), the performance are improved comparing to that of the fixed PID control system (for CPTC system - e_{max}: 9.32 μm → 7.91 μm).

Fig. 16. shows the corresponding experimental results from the 20 kHz drive frequency to 35 kHz. From Figs. 12 and 16, the fixed PID controller on each drive frequency is not acceptable for the reason of the overshoot and the maximum tracking error deteriorations.

From these results, it can be confirmed that the control performance can be guaranteed by the gain-scheduled control method.

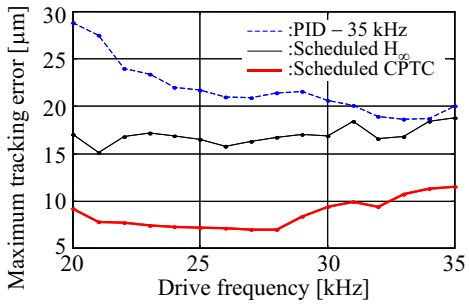

Fig. 16. Experimental results of the maximum tracking error to the ramp position reference.

4.2 Gain-Scheduled Control

Taking into consideration that the lower drive frequency is used as much as possible as described before, the scheduling strategy of α is assumed with respect to the velocity reference v^{ref} as shown in Fig.17. $v^{ref}_{\omega min}$ and $v^{ref}_{\omega max}$ represent the maximum velocity reference with the drive frequency ω_{min} and ω_{max}, respectively. In this case 80 % of the velocity is assumed as- $v^{ref}_{\omega min}$:26.9 mm/s($= k_{min} \times 130\ V \times 0.8$), $v^{ref}_{\omega max}$:75.2 mm/s($= k_{max} \times 130\ V \times 0.8$).

On slip-less drive(Egashira *et al.*, 2004), the applied force F_a by the SPIDER may not exceed the frictional force F_f of the contacting plate as:

$$F_a \leq F_f, \quad F_a = ma,\ F_f = \mu N \tag{13}$$

with the condition: $a = r\dot{\omega}$, where m is the mass of the stage (1.0 kg), a is the acceleration of the stage, μ is a friction coefficient of the plate(0.3), N is the preload force vertical to the plate (40 N) and r is radius of gyration of the actuator ($660{\cdot}10^{-12} \cdot 4 \cdot 260/2$). This condition can result in the rate restriction of α for the scheduling of Fig.17 as:

$$\dot{\alpha} = \frac{\partial \alpha}{\partial \omega} \cdot \frac{d\omega}{dt} \leq \frac{1}{\omega_{min} - \omega_{max}} \cdot \frac{\mu N}{mr} \tag{14}$$

In order to assure the slip-less drive, according with the investigated system, the variation rate of the frequency must be limited as $|\dot{\alpha}|_{max} \leq 371$.

Taking this condition into consideration, the differentiable velocity reference, that is, the velocity S-profile reference as shown in Fig.18 is applied.

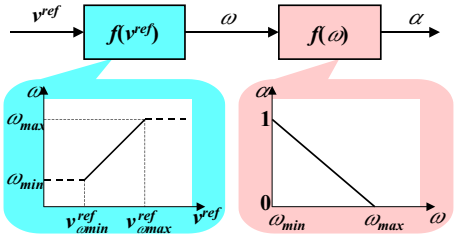

Fig. 17. Scheduling strategy with respect to velocity reference.

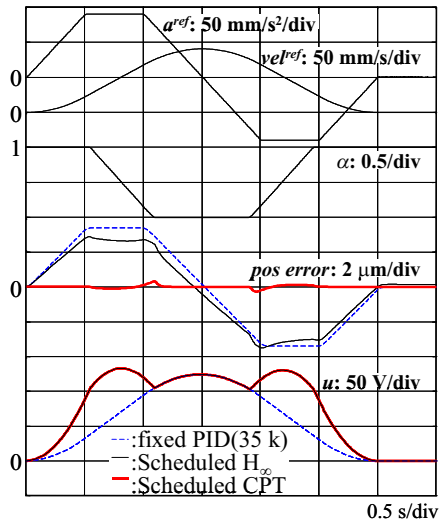

Fig. 18. Time responses of variable frequency control.

Fig.18 also illustrates the time responses of the various signals (only in this case simulation results are presented). It can be confirmed that the gain scheduling is well performed.

5. CONCLUSION

In this paper, the novel control method of the SPIDER-driven precision stage considering the drive-frequency characteristic is discussed. In order to assure the continuous-path tracking and the slip-less drive, the gain-scheduled control considering the drive-frequency change is adopted.

The effectiveness of the proposed control method is verified through simulations and the experiments.

REFERENCES

Doyle, J. C., B. A. Francis and A. R. Tannenbaum (1992). *Feedback Control Theory*. Macmillan. New York.

Egashira, Y., H. Furukawa, T. Endo, K. Kosaka, A. Nakada, H. Kubota and T. Ohmi (2004). Development of the non-resonant ultrasonic motor driving method using static friction area-. *The 16th symposium on Electromagnetics and dynamics(SEAD16)* pp. 313–316.

Gahinet, Pascal (1995). *Matlab - LMI Control Toolbox User's Guide*. MathWorks, Inc.

Goodwin, G. C., S. F. Graebe and M. E. Salgado (2001). *Control System Design*. Prentice Hall. New Jersey.

Hashimoto, S., K. Ohishi, T. Ohishi, T. Ishikawa adn K. Kosaka, Y. Egashira, H. Kubota and T. Ohmi (2004). Ultra-precision stage control based on friction model of non-resonant ultrasonic motor. *Proc. of AMC'04* pp. 559–564.

Ljung, L. (1999). *System Identification -Theory for the User (2nd edition)*. Prentice Hall. New Jersey.